Cell PRESS
Open ACCESS

SUPPLEMENTAL REFERENCES

Aleshin, A.E., Schraufstatter, I.U., Stec, B., Bankston, L.A., Liddington, R.C., and Discipio, R.G. (2012). Structure of Complement C6 suggests a mechanism for initiation and unidirectional, sequential assembly of the Membrane Attack Complex (MAC). J. Biol. Chem.

Collaborative Computational Project, Number 4. (1994). The CCP4 suite: programs for protein crystallography. Acta Crystallogr. D Biol. Crystallogr. *50*, 760–763.

Fredslund, F., Laursen, N.S., Roversi, P., Jenner, L., Oliveira, C.L., Pedersen, J.S., Nunn, M.A., Lea, S.M., Discipio, R., Sottrup-Jensen, L., and Andersen, G.R. (2008). Structure of and influence of a tick complement inhibitor on human complement component 5. Nat. Immunol. *9*, 753–760.

Heymann, J.B., and Belnap, D.M. (2007). Bsoft: image processing and molecular modeling for electron microscopy. J. Struct. Biol. *157*, 3–18.

Janssen, B.J., Huizinga, E.G., Raaijmakers, H.C., Roos, A., Daha, M.R., Nilsson-Ekdahl, K., Nilsson, B., and Gros, P. (2005). Structures of complement component C3 provide insights into the function and evolution of immunity. Nature *437*, 505–511.

Janssen, B.J., Christodoulidou, A., McCarthy, A., Lambris, J.D., and Gros, P. (2006). Structure of C3b reveals conformational changes that underlie complement activity. Nature *444*, 213–216.

Lovelace, L.L., Cooper, C.L., Sodetz, J.M., and Lebioda, L. (2011). Structure of human C8 protein provides mechanistic insight into membrane pore formation by complement. J. Biol. Chem. *286*, 17585–17592.

Mollnes, T.E., Lea, T., Harboe, M., and Tschopp, J. (1985). Monoclonal antibodies recognizing a neoantigen of poly(C9) detect the human terminal complement complex in tissue and plasma. Scand. J. Immunol. *22*, 183–195.

Nagar, B., Jones, R.G., Diefenbach, R.J., Isenman, D.E., and Rini, J.M. (1998). X-ray crystal structure of C3d: a C3 fragment and ligand for complement receptor 2. Science *280*, 1277–1281.

Pettersen, E.F., Goddard, T.D., Huang, C.C., Couch, G.S., Greenblatt, D.M., Meng, E.C., and Ferrin, T.E. (2004). UCSF Chimera—a visualization system for exploratory research and analysis. J. Comput. Chem. *25*, 1605–1612.

Scheres, S.H., Núñez-Ramírez, R., Sorzano, C.O., Carazo, J.M., and Marabini, R. (2008). Image processing for electron microscopy single-particle analysis using XMIPP. Nat. Protoc. *3*, 977–990.

Slade, D.J., Lovelace, L.L., Chruszcz, M., Minor, W., Lebioda, L., and Sodetz, J.M. (2008). Crystal structure of the MACPF domain of human complement protein C8 alpha in complex with the C8 gamma subunit. J. Mol. Biol. *379*, 331–342.

Tang, G., Peng, L., Baldwin, P.R., Mann, D.S., Jiang, W., Rees, I., and Ludtke, S.J. (2007). EMAN2: an extensible image processing suite for electron microscopy. J. Struct. Biol. *157*, 38–46.

van den Elsen, J.M., Martin, A., Wong, V., Clemenza, L., Rose, D.R., and Isenman, D.E. (2002). X-ray crystal structure of the C4d fragment of human complement component C4. J. Mol. Biol. *322*, 1103–1115.

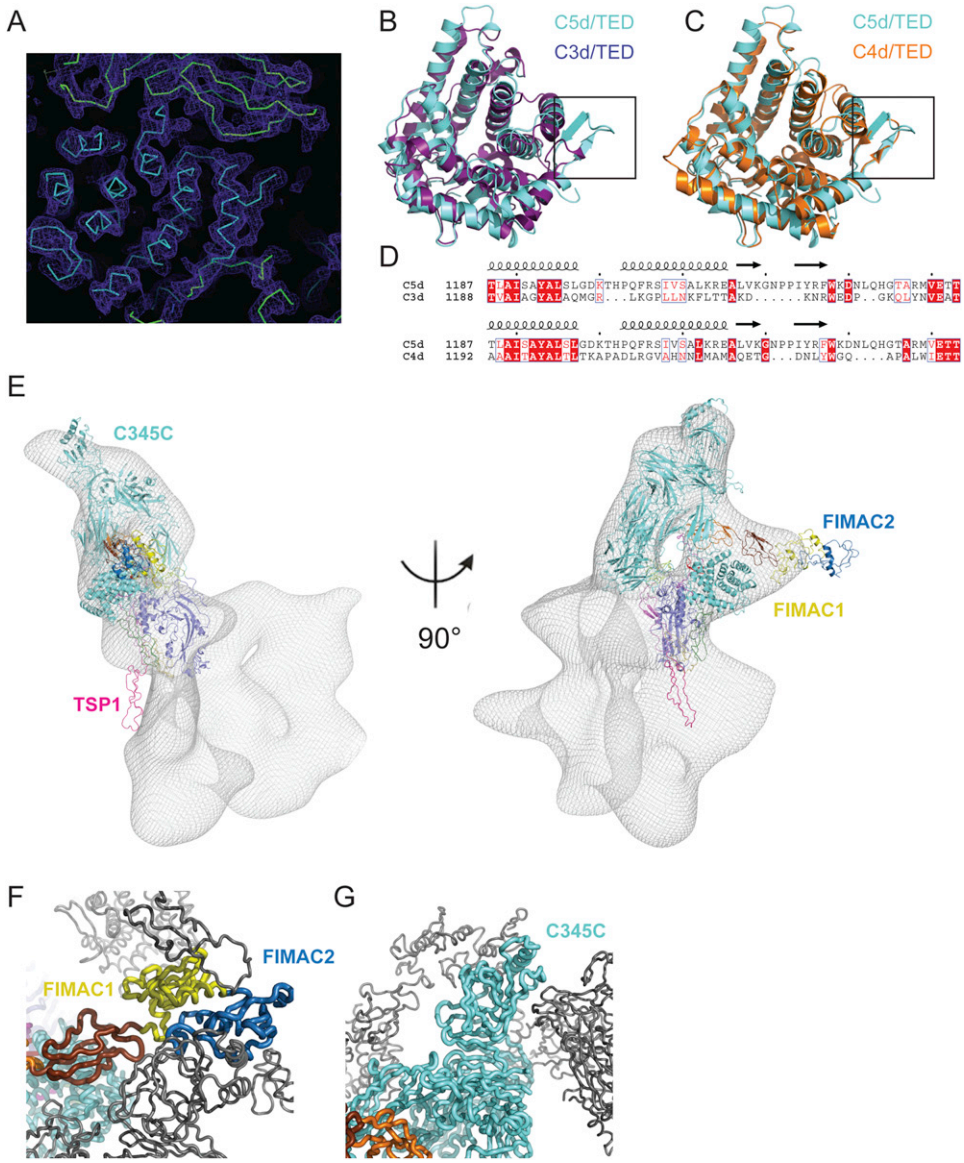

Figure S1. Crystal Structure of C5b6, Related to Figure 1

(A) An example of electron density of C5b6. A 2mFo-DFc (φ_{calc}) map contoured at 1.1σ showing the interface between C5d/TED (cyan) and the CCP domains of C6 (green).

(B) Structure-based comparison of C5d with C3d. C5d (cyan) is superimposed on C3d (Nagar et al., 1998)(PDB code: 1C3D, purple).

(C) Structure based comparison of C5d with C4d. C5d (cyan) is superimposed on C4d (van den Elsen et al., 2002)(PDB code: 1HZF, orange). The boxes indicate the β-hairpin insertion in C5d that interacts with the linker region of C6.

(D) Structure-based sequence alignments between C5 and C3 (top) and C5 and C4 (bottom) of the region that contains the β-hairpin insertion. The secondary structure of C5d is indicated above each sequence, with black dots marking 10-residue increments.

(E) Docking of the C5b6 crystal structure defined the identity of the sC5b9 protrusion. Although the conformation of the C5b6 core (colored as in Figures 1 and 2) was in agreement with the cryo-EM map (gray mesh), the extreme N- and C-terminal domains (TSP1, magenta; FIMAC1, yellow; and FIMAC2, dark blue) lie outside the density. The resolution of the reconstruction restricted our interpretation of these domains in the context of the complex, therefore we have excluded them from our sC5b9 model. In addition, the C345C domain of C5b, known to be flexible (see Figure 1D), is also partially out of density when C5b6 is docked as a single rigid body.

(F and G) An analysis of symmetry-related molecules in the C5b6 crystal structure (gray ribbons) suggest that their orientations could be influenced by crystal packing.

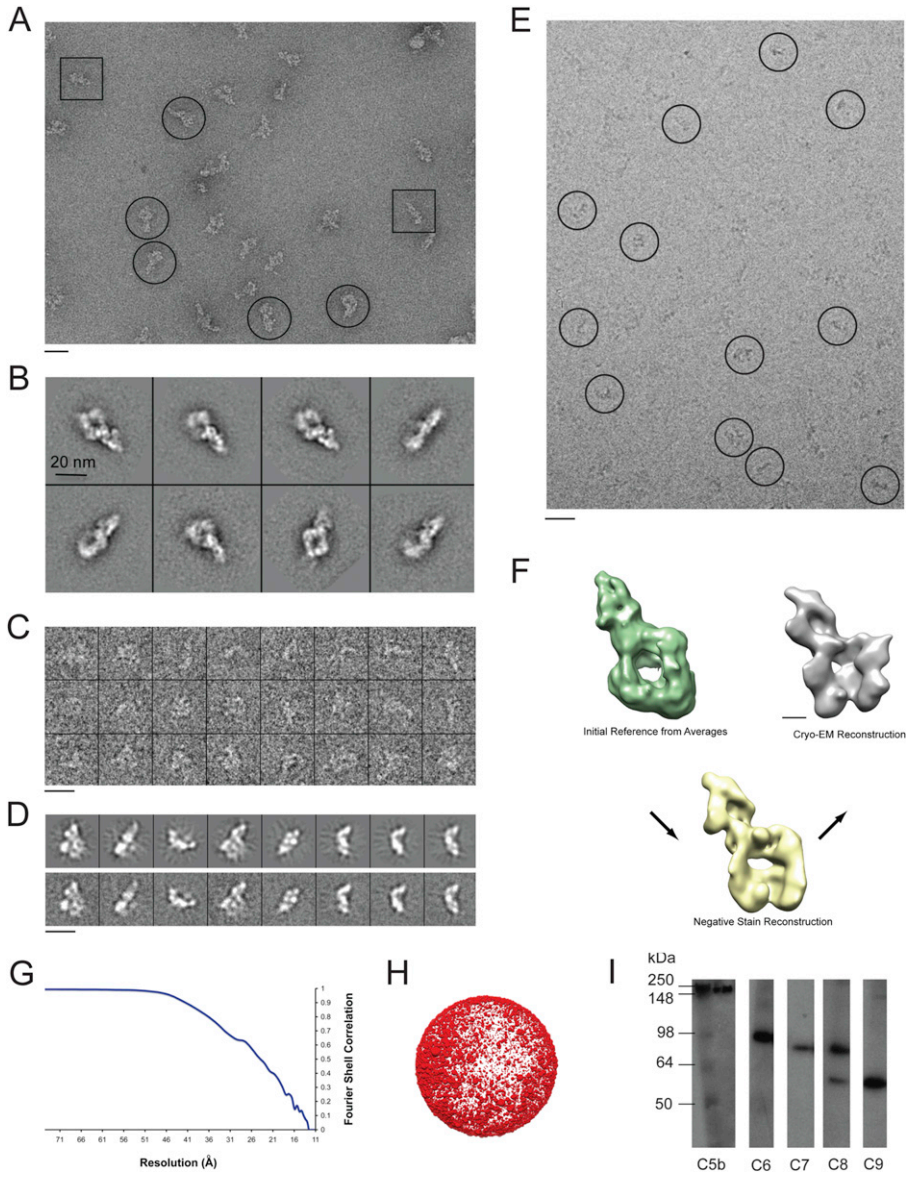

Figure S2. Electron Microscopy of sC5b9, Related to Figure 3

(A) A typical micrograph of negatively stained sC5b9 complexes reveals mono-dispersed molecules in a range of orientations. Characteristic "top" views (highlighted within circles) show a square-like core region with a large protrusion, assigned to C5b6. sC5b9 views from the side (highlighted within squares) appear as elongated thin objects. Scale bar, 45 nm.

(B) Single images of sC5b9 extracted from the micrographs were subjected to reference-free classification strategies. Resulting reference-free averages reveal several distinct views of the complex. Scale bar, 20 nm.

(C) Gallery of cryo-EM 2D images. Scale bar, 30 nm.

(D) Two-dimensional projections of the sC5b9 cryo-EM reconstruction (top panel) were compared with averages of raw images (bottom panel). Scale bar, 30 nm.

(E) Cryo-electron micrograph of sC5b9. Individual particles are circled. Scale bar, 60 nm.

(F) To minimize distortions of the structure, a Gaussian blob was used as references to initiate Euler angular assignment of negative stain reference-free generated class averages in EMAN2 (Tang et al., 2007). The resulting reconstruction (green) was then used as a template for the refinement of negatively stained sC5b9 single particles. Upon convergence, the negative stain reconstruction (yellow) served as a reference for the alignment of cryo-EM data in Xmipp (Scheres et al., 2008). The final cryo-EM reconstruction is shown in gray. Scale bar, 60 Å.

(G) The final resolution of the sC5b9 reconstruction, 24 Å, was assessed using the Fourier shell correlation with a cutoff of 0.5.

(H) The angular distribution of particle orientations was plotted in three dimensions using Chimera (Pettersen et al., 2004). Spheres represent unique orientations, where the size of the sphere is proportional to the number of particles assigned to a given set of angles.

(I) A non-reduced denaturing SDS-PAGE gel was run of the imaged sample and transferred to a nitrocellulose membrane for Western blot analysis. Polyclonal antibodies against C5b, C6, C7, C8 and C9 were used to probe the presence of MAC components in the complex. As expected, C8 runs as two bands: C8β (64kDa) and the C8αγ disulfide-linked heterodimer (86kDa).

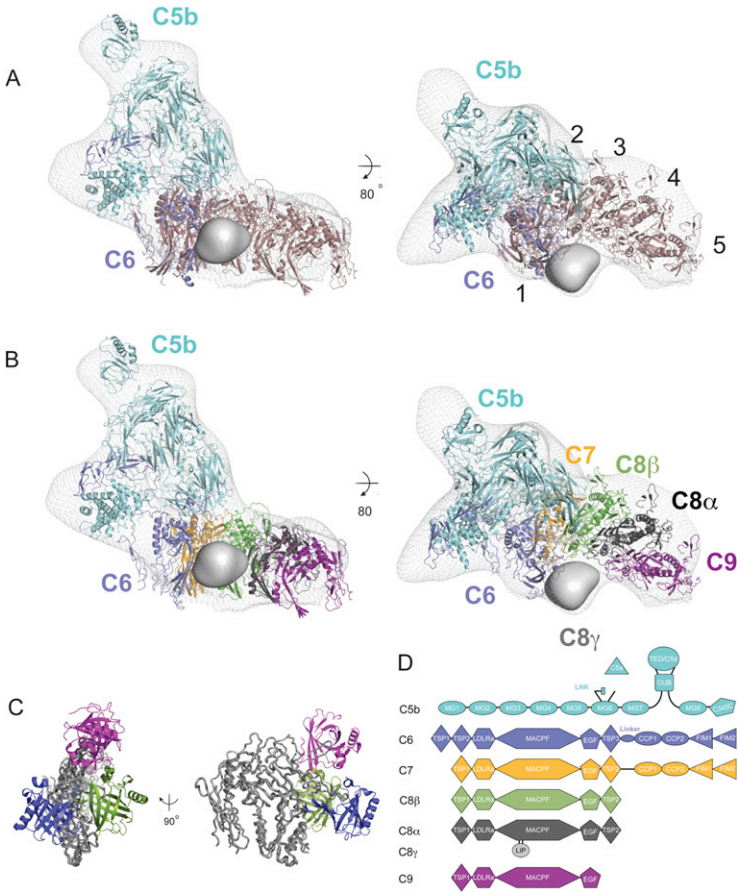

Figure S3. Pseudo Atomic Modeling of sC5b9 MAC Components, Related to Figure 3

The cryo-EM sC5b9 reconstruction was divided into two sections using the watershed method for segmentation in Chimera (Pettersen et al., 2004). Anti-C9 antibody labeling identified the segment containing MAC components, which was then used for all subsequent docking experiments (gray mesh).

(A) The C5b6 crystal structure (C5b, cyan; C6, blue) was manually placed in the density and rigid-body refined in Chimera. The real space correlation coefficient between the map and the C5b6 model was calculated to be 0.85 using Bsoft (Heymann and Belnap, 2007). A model for 5 MACPF domains and their flanking TSP, LDLRa, and EGF domains was constructed based on the MACPF-MACPF interaction in the C8 crystal structure (Lovelace et al., 2011) (pink); MACPF transmembrane segments were not included. This model was independently fit into the arc-shaped crescent of the reconstruction and refined as a single rigid body (correlation coefficient of 0.88). Overlaying the 5 MAC model (numbered 1-5) with the fitting of C5b6 showed that the majority of the C6 MACPF domain overlapped with the first MACPF in the arc.

(B) Sequential iterative refinement of C5b6, a 4 MACPF model (colored as in Figure 3), and the crystal structure of C8γ (Lovelace et al., 2011) (gray density) resulted in a correlation coefficient of 0.89.

(C) Crystal structures of C8αγ from the C8αγ complex alone (Slade et al., 2008) (PDB code: 2RD7) (C8γ, blue) and from the C8αγβ complex (Lovelace et al., 2011) (PDB code: 3OYJ) (C8γ, green) were superposed based on the C8α subunit (gray) and compared with the location of C8γ in the sC5b9 complex (magenta). Together, the three structures show a range conformations enabled by a flexible hinge in the C8α hairpin, which extends from the core MACPF domain.

(D) Schematic representation of the domain composition for MAC proteins in sC5b9. C5b is composed of 8 macroglobulin domains (MG1-MG8), a CUB domain, a thioester containing domain (C5d/TED), an extended linker region, and a C-terminal C345C domain. Not present in C5b, the anaphylotoxin (C5a) that results from C5 cleavage is indicated in red. C6 and C7 share a similar domain architecture consisting of thrombospondin type 1 (TSP), low-density lipoprotein receptor type A (LDLRa), membrane attack complex perforin fold (MACPF); epidermal growth factor (EGF), complement control protein (CCP), and factor I-like modules (FIM). C8 is composed of 3 subunits: C8α, C8β and C8γ, of which C8γ forms a disulfide bond with a hairpin extension of C8α-MACPF. Both C8α and C8β share homologous TSP, LDLRa, MACPF and EGF domains, while C8γ has a lipocalin (Lip) fold. C9 also contains TSP, LDLRa, MACPF, EGF modules.

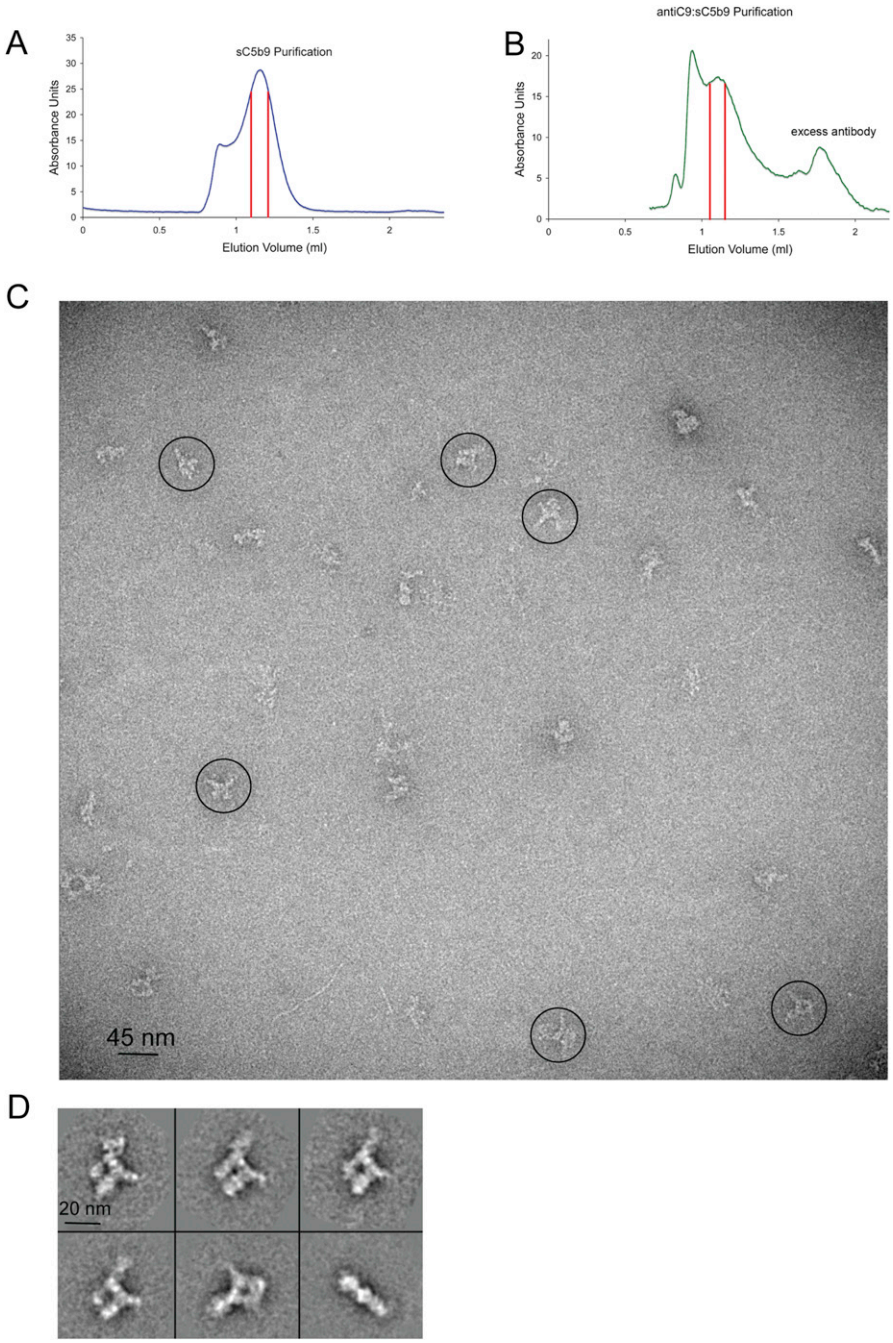

Figure S4. Antibody Labeling of sC5b9 Complexes, Related to Figure 3

(A) sC5b9 was purified by size-exclusion chromatography. The elution profile (blue curve) from a Superose 6 PC 3.2/30 gel filtration column is shown. Absorbance units were recorded at a wavelength of 280 nm. Red lines indicate the fraction collected.

(B) Purified sC5b9 (from the pooled fraction indicated in panel A) was incubated with excess aE11, a monoclonal antibody against the neo-antigen of C9 present in both sC5b9 and the MAC (Mollnes et al., 1985). Complexes were separated from unbound antibody by an additional purification before imaging. Although the addition of antibody resulted in increased higher order oligomers, immune-labeled sC5b9 complexes could be separated from the aggregate and excess antibody, which eluted at 1.8mls. The elution profile from Superose 6 PC 3.2/30 gel filtration column is indicated (green curve). The fraction used for imaging is marked by red lines.

(C) Micrographs of negatively stained sC5b9 immune-complexes reveal molecules with a distinctive decoration. This extra density was specific to the addition of the anti-C9 neo-antibody and thus mapped the location of this subunit. Typical immune-complexes are highlighted within circles. Scale bar, 45 nm.

(D) Reference-free averages of the sC5b9 immune-complexes confirmed the presence of a density corresponding to the labeling of the C9 subunit at the opposite end of the C5b6 protrusion. Scale bar, 20 nm.